HETEROCYCLES, Vol. 95, No. 2, 2017, pp. 1030-1040. © 2017 The Japan Institute of Heterocyclic Chemistry
Received, 13th September, 2016, Accepted, 24th October, 2016, Published online, 27th December, 2016
DOI: 10.3987/COM-16-S(S)75

REVERSIBILITY OF 3-PHENYL-2-OXINDOLE DIMER FORMATION: APPLICATION TO CONSTRUCT COMPOUNDS WITH TWO DISTINCT VICINAL ALL-CARBON QUATERNARY CENTERS

Yoshihiro Sohtome,[1,2]* Masumi Sugawara,[1] Daisuke Hashizume,[3] Daiki Hojo,[2] Miki Sawamura,[1] Atsuya Muranaka,[2,4] Masanobu Uchiyama,[2,4] and Mikiko Sodeoka[1,2]*

[1] Synthetic Organic Chemistry Laboratory, RIKEN, 351-0198, Japan. [2] RIKEN Center for Sustainable Resource Science, 351-0198, Japan. [3] RIKEN Center for Emergent Matter Science, 351-0198, Japan. [4] Elements Chemistry Laboratory, RIKEN, 351-0198, Japan; E-mail: sohtome@riken.jp, sodeoka@riken.jp

Dedicated to Professor Dr. Masakatsu Shibasaki on the occasion of his 70th birthday

Abstract – Here we describe the critical role of the C(3) phenyl ring in providing selective access to the *meso*-dimer of *N*-Boc-3-phenyl-2-oxindole, which contains two contiguous all-carbon quaternary centers. Solid-state analysis of the *meso*-dimer suggested that weak CH/O and CH/π interactions cooperatively decrease the energy of the ground state in the (±)-*sc* (*synclinal*) conformation. Solution-state analyses and DFT calculations revealed that the C(3)–C(3') σ-bond of the *meso*-dimer is labile, and the phenyl group at the C(3) position makes a key contribution to stabilizing the monomeric radical species. Based on these findings, we developed a facile radical-based transformation of the *meso*-dimer to construct a variety of compounds with two distinct contiguous all-carbon centers.

INTRODUCTION

Molecules containing contiguous all-carbon quaternary centers display characteristic biological activities.[1] The congested nature of the structural motif presents a synthetic challenge, and chemists have sought an efficient strategy to construct such centers, focusing mainly on the steric parameters.[2] During our studies on chaetocin and its synthetic derivatives, which are histone methyltransferase inhibitors,[3] we became interested in the conformational characterization of 3,3'-substituted 2,2'-oxindole dimers,[4–7] and

in their potential as precursors for constructing two distinct vicinal all-carbon quaternary centers.

Specifically, we found inspiration from two reported features of the dimers **2** derived from 2-oxindoles **1** (Scheme 1). First, the diastereoselectivity (*dl* vs. *meso*) is generally variable depending on the substituent at the C(3) position in the process of oxidative[4a-g,4k] or photocatalytic dimerization,[5] regardless of the protecting group on nitrogen and the reaction conditions (solvent, oxidant, temperature, *etc*.). For example, the reactions of 3-alkyl-substituted-2-oxindoles give the dimers with low selectivity (*dl*:*meso*). In sharp contrast, *meso*-dimers are formed as the major product when 3-aryl-substituted-2-oxindoles are used as precursors.[4i] Second, the C(3)–C(3') σ-bond length of the dimers **2** (3-alkyl-substituted dimer, 1.565–1.597 Å;[4d-f,h,5,7] 3-aryl-substituted dimer, 1.610 Å[4i]) is greater than the typical C(sp^3)–C(sp^3) bond length [1.530(15) Å].[8] The unusual elongation of the σ-bond in the dimer suggests a weak bond dissociation energy (BDE). Nevertheless, the substituent effect on the diastereoselectivity in the oxidative dimer-forming reaction of **1** remains unclear; only a conformational analysis of *dl*- and *meso*-dimers bearing a methyl group at the C(3) position in the solution state has been reported.[4d] Here we describe our investigations on the influence of the phenyl group at the C(3) position; we show that this group plays a critical role in decreasing the BDE of **2a**, leading to selective formation of *meso*-dimer **2a** from *N*-Boc-3-phenyl-2-oxindole **1a**. Solid- and solution-state analyses, together with theoretical calculations, reveal that this phenyl group participates in stabilizing the monomeric carbon radical species, providing evidence that *dl*-**2a** and *meso*-**2a** are interconvertible.[9] Since multiple weak intramolecular CH/O[10] and CH/π interactions[11] make *meso*-**2a** more thermodynamically stable, it is the major product in the oxidative dimerization reaction. On the basis of the observed lability of the C(3)–C(3') σ-bond in **2a**, we also show that the *meso*-dimer **2a** can be employed for radical-based construction of two distinct contiguous all-carbon quaternary centers.

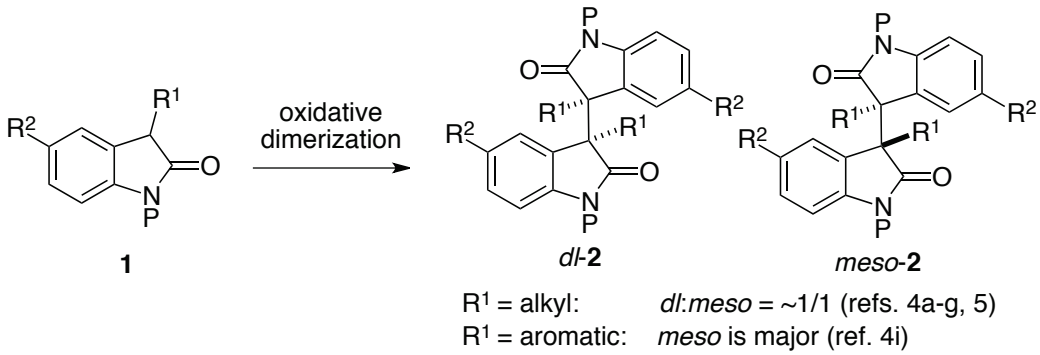

Scheme 1. Oxidative dimerization of **1**; the ratio of *dl*-**2**:*meso*-**2** is generally variable depending on the R^1 group.

RESULTS AND DISCUSSION

We began this investigation by preparing the requisite dimer **2a** from *N*-Boc-3-phenyl-2-oxindole **1a**, based on the reported procedure.[12] The reaction of **1a** using a stoichiometric amount of $K_3[Fe(CN)_6]$ and

KOH aq. in CCl_4 promoted oxidative C(sp^3)–C(sp^3) bond formation at the C(3) position, affording the corresponding dimer.[4a,c,d,i] Single-crystal X-ray diffraction structural analysis of the major product unambiguously revealed that **2a** is the *meso*-dimer, and the (±)-*sc* (*synclinal*) conformation is predominant.[4d-f,h,i,5,7] The (±)-*sc* conformation is stabilized by multiple weak intramolecular CH/O and CH/π interactions, in which the phenyl rings participate: C(7)–H···O(1): 2.263 Å, C(15)–H···O(3): 2.237 Å, C(7')–H···O(1'): 2.351 Å, C(15')–H···O(3'): 2.394 Å, C(5)–H···Ph: 2.742 Å, C(5')–H···Ph in the oxindole core: 2.598 Å. The major difference between *meso*-**2a** and *meso*-**2b** (R^1 = 4-F-C_6H_4-, R^2 = H, P = Boc) as reported by Gade[4i] is the number of CH/π interactions, presumably reflecting the difference of electron density on the aromatic ring at the C(3) position (Ph *vs*. 4-F-C_6H_4-); two distinct CH/π interactions are involved in *meso*-**2a**, while only one CH/π interaction is present in *meso*-**2b**. These results can be well explained by the typical tendency of an electron-rich π system to interact more strongly with C–H bonds.[11] The torsion angle between phenyl groups C(14) and C(14') in *meso*-**2a**, viewed from C(3) to C(3'), also becomes larger than those of *meso*-**2b** [*meso*-**2a**: –69.32(11)°, *meso*-**2b**: –56.97(14)°], likely due to the additional CH/π interaction. The σ-bond between C(3)–C(3') in *meso*-**2a** is also significantly longer than that in *meso*-**2b** [*meso*-**2a**: 1.6194(14) Å, *meso*-**2b**: 1.6097(18) Å].[4i]

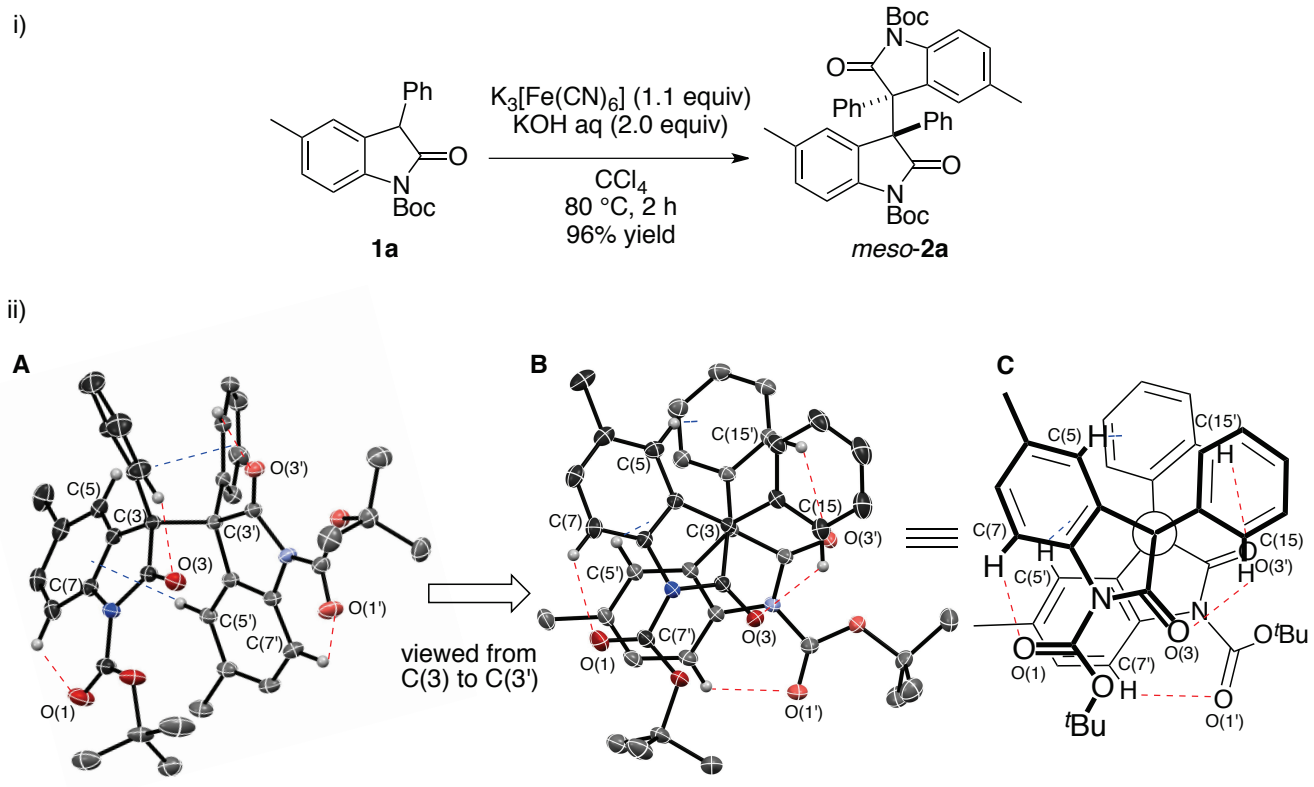

Scheme 2. i) Procedure for synthesis of *meso*-**2a**; ii-A) and ii-B) ORTEP drawings (50% probability ellipsoids) of *meso*-**2a**, ii-C) the chemical structure of *meso*-**2a** viewed from C(3) to C(3'); CH/O interactions are represented by red broken lines, while CH/π interactions are represented by blue broken lines. Only hydrogen atoms associated with CH/O and CH/π interactions are shown, for the sake of clarity.

Next, we characterized the conformation of *meso*-**2a** and the nature of the C(3)–C(3') σ-bond in the solution state (Figure 1). The existence of intramolecular CH/π interactions in *meso*-**2a** is evident from the high-field shift in ^{1}H NMR, in which two protons were observed as a broad singlet at 5.89 ppm in $CDCl_3$ at room temperature. The unique shift can be explained by the ring current effect, and is consistent with the idea that (±)-*sc* conformation predominates even in $CDCl_3$. Although *meso*-dimer **2a** is stable at room temperature, the generation of the carbon radical from *meso*-**2a** can be dynamically monitored by measuring changes in the absorptions in the ultraviolet and visible regions in response to temperature change.[13] The absorbances at 342 and 520 nm gradually increased as the temperature was increased (Figure 1-ii). When the temperature was again decreased to 25 °C, the spectra showed good agreement with the original spectrum measured at 25 °C, indicating the reversible nature of dimer **2a** formation from the corresponding carbon radical species.[9]

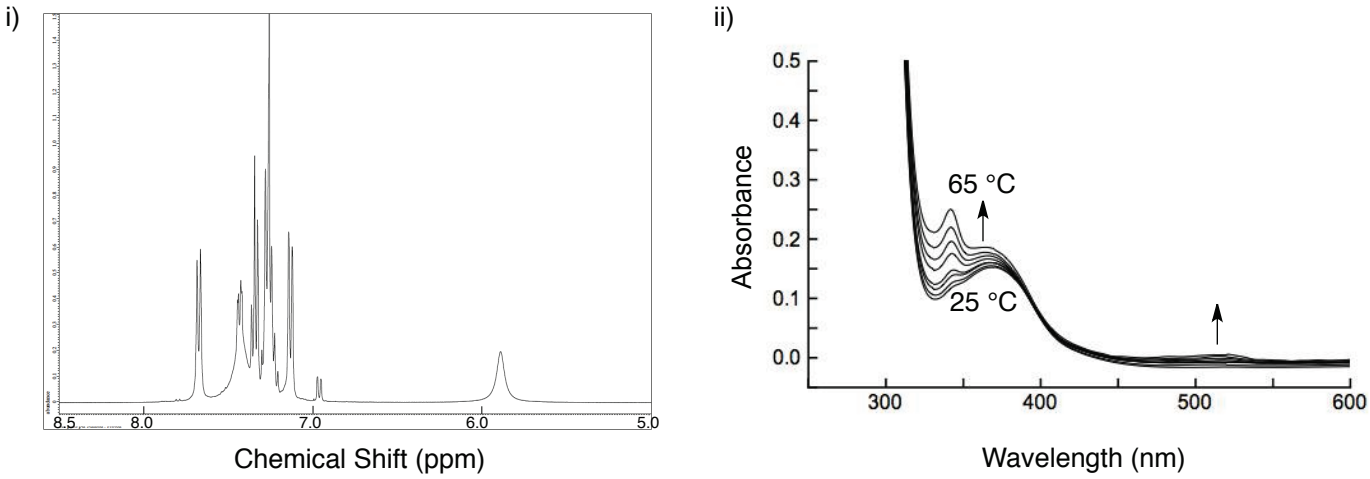

Figure 1. i) ^{1}H NMR spectrum of *meso*-**2a** ($CDCl_3$); ii) absorption spectra of *meso*-**2a** at different temperatures in $CHCl_3$ (4 mM).

To better understand the restricted rotation and the features of the carbon radical species derived from *meso*-**2a** by comparison with the experimentally obtained NMR and UV-Vis spectra (Figure 1), we performed density functional theory (DFT) calculations[14] on *meso*-**2a** using the M06-2X functional[15] with the 6-311G(d,p) basis set. Partial geometry optimization by varying the dihedral angle (ω) of C(14)–C(3)–C(3')–C(14') by 20° jumps followed by unconstrained optimization gave two optimized structures, including **DFT-*meso*-2aI** as a (±)-*sc* conformer with ω = –63.35, 63.35° and **DFT-*meso*-2aII** as an *ap* (*antiperiplanar*) conformer with ω = 163.51° (see Supporting Information for details). The energy value of **DFT-*meso*-2aII** (ΔG_{II-I} = 2.8 kcal/mol) is higher than that of **DFT-*meso*-2aI**, indicating that the population of **2aI** should be larger than that of **2aII**. The simulated ^{1}H NMR spectra of **DFT-*meso*-2aI**, involving CH/π interactions, reproduced well the observed characteristic high-field shifts owing to the

ring current effect, which afforded two peaks at 6.26 and 5.47 ppm; C(5')–H is observed at higher field (5.47 ppm) than C(5)–H (6.26 ppm). These results are well correlated with the distance differences in the CH/π interactions; the distance between C(5')–H and the electron-rich oxindole (2.489 Å) is shorter than that between C(5)–H and the phenyl group (2.641 Å). In sharp contrast to **DFT-*meso*-2aI**, the simulated ^{1}H NMR spectrum of **DFT-*meso*-2aII** gives no such high field shift. Thus, the observed ^{1}H NMR experiments and computational investigations support the idea that the (±)-*sc* conformation, as shown in **DFT-*meso*-2aI**, involving the intramolecular CH/π interactions of C(5)–H and C(5')–H, is retained even in the solution state.

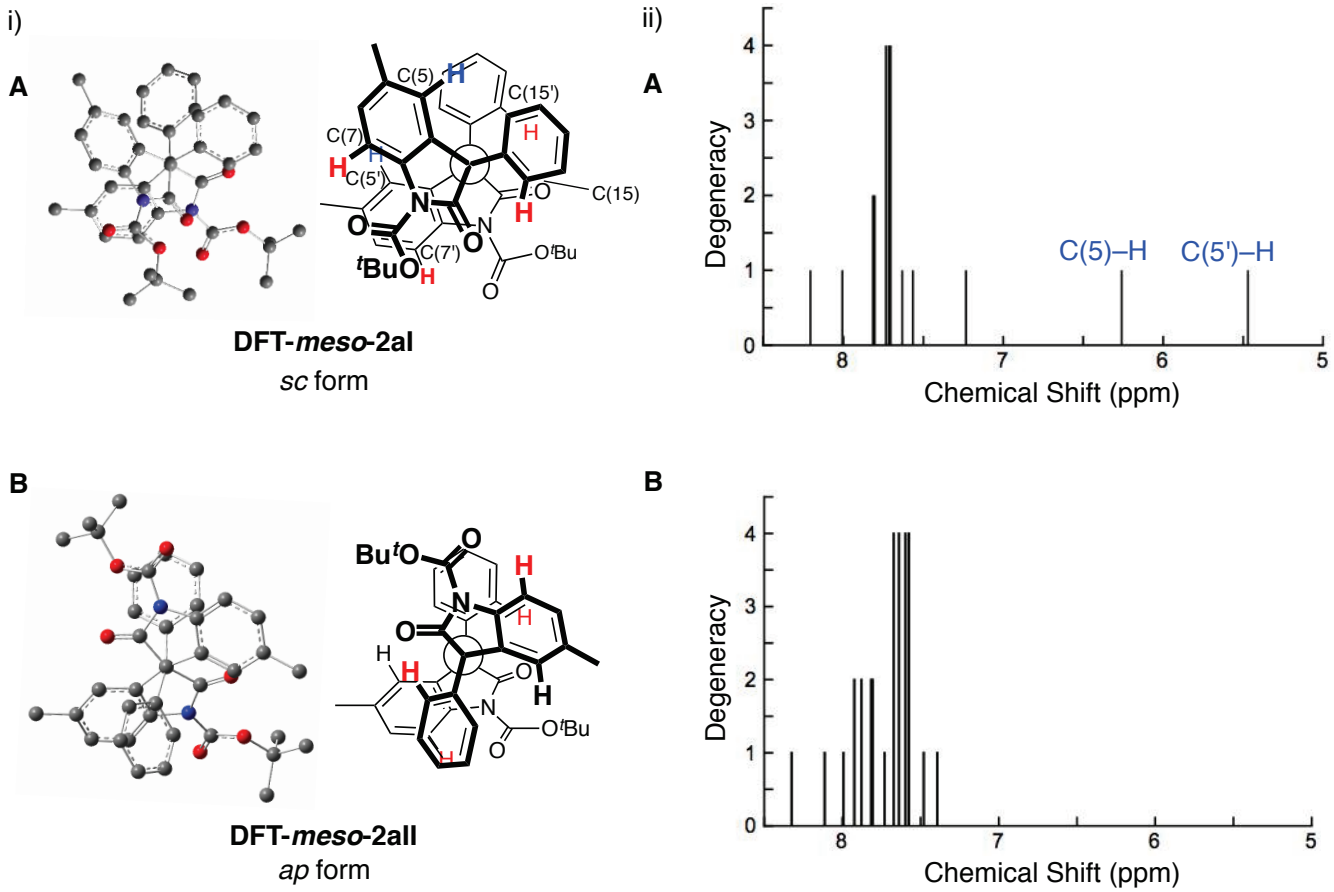

Figure 2. i) The optimized structures of **2aI** and **2aII**; ii) the simulated NMR spectra of **2aI** and **2aII**. All hydrogen atoms in ball illustrations are omitted for the sake of clarity.

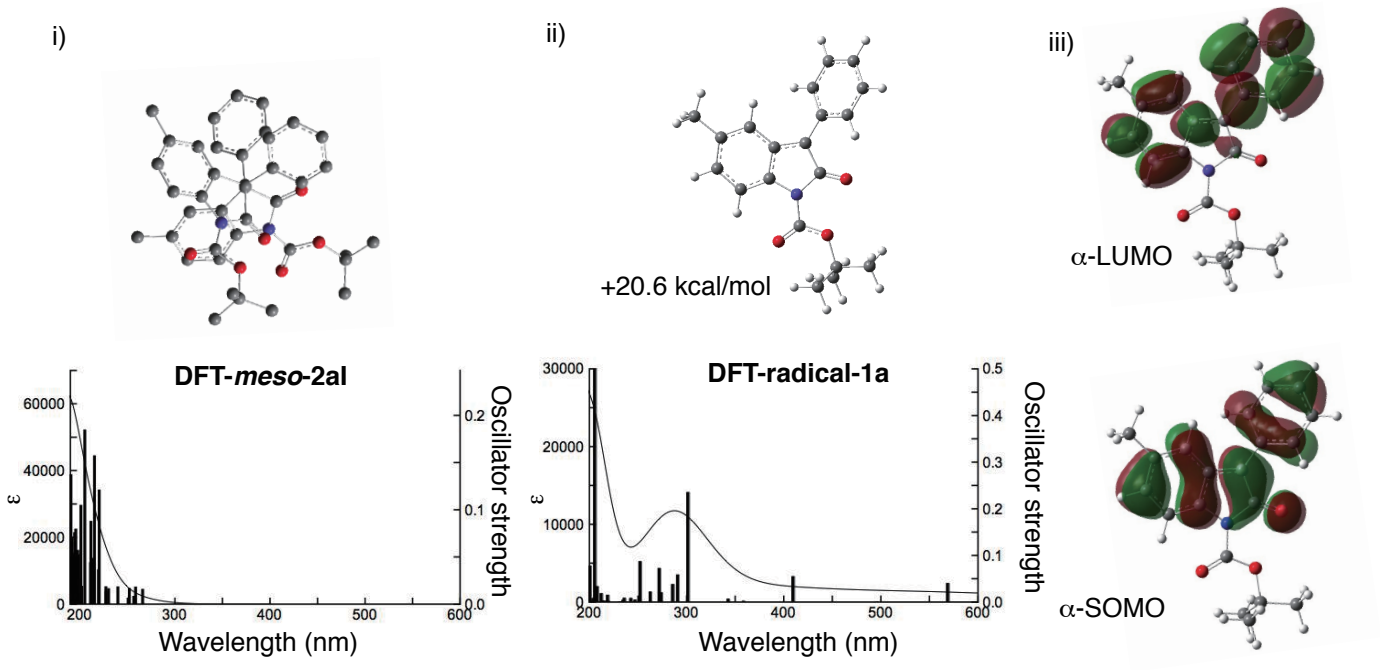

Figure 3. The simiulated UV-Vis spectra (σ = 0.5 eV) for i) **DFT-*meso*-2aI** computed at the M06-2X/6-311G(d,p) level of theory and ii) **DFT-radical-1a** computed at the UM06-2X/6-311G(d,p) level of theory; iii) Kohn–Sham orbitals of α-LUMO and α-SOMO in **DFT-radical-1a**. All hydrogen atoms for **DFT-*meso*-2aI** in ball illustrations are omitted for the sake of clarity.

The observed UV-Vis spectrum (Figure 1-ii) can also be reproduced from the simulated UV-Vis spectra of **DFT-*meso*-2aI** and **DFT-radical-1a** (Figure 3). For example, only weak electronic transitions (oscillator strength f<0.1) at the range over 220 nm were predicted for **DFT-*meso*-2aI** (Figure 3-i). In contrast, not only the strong intensity at 302 nm, but also weak intensities at 410 and 569 nm in **DFT-radical-1a** were obtained (Figure 3-ii). The dominant contribution (62.6%) of the electronic transition at 302 nm in the calculated UV-Vis spectrum in **DFT-radical-1a** was found to be associated with α-SOMO → α-LUMO, in which the electron is delocalized on the oxindole core and the 3-phenyl group (Figure 3-iii). These solution-state analyses and DFT simulations highlight the key contribution of the 3-phenyl group in stabilizing the radical species derived from *meso*-**2a**.

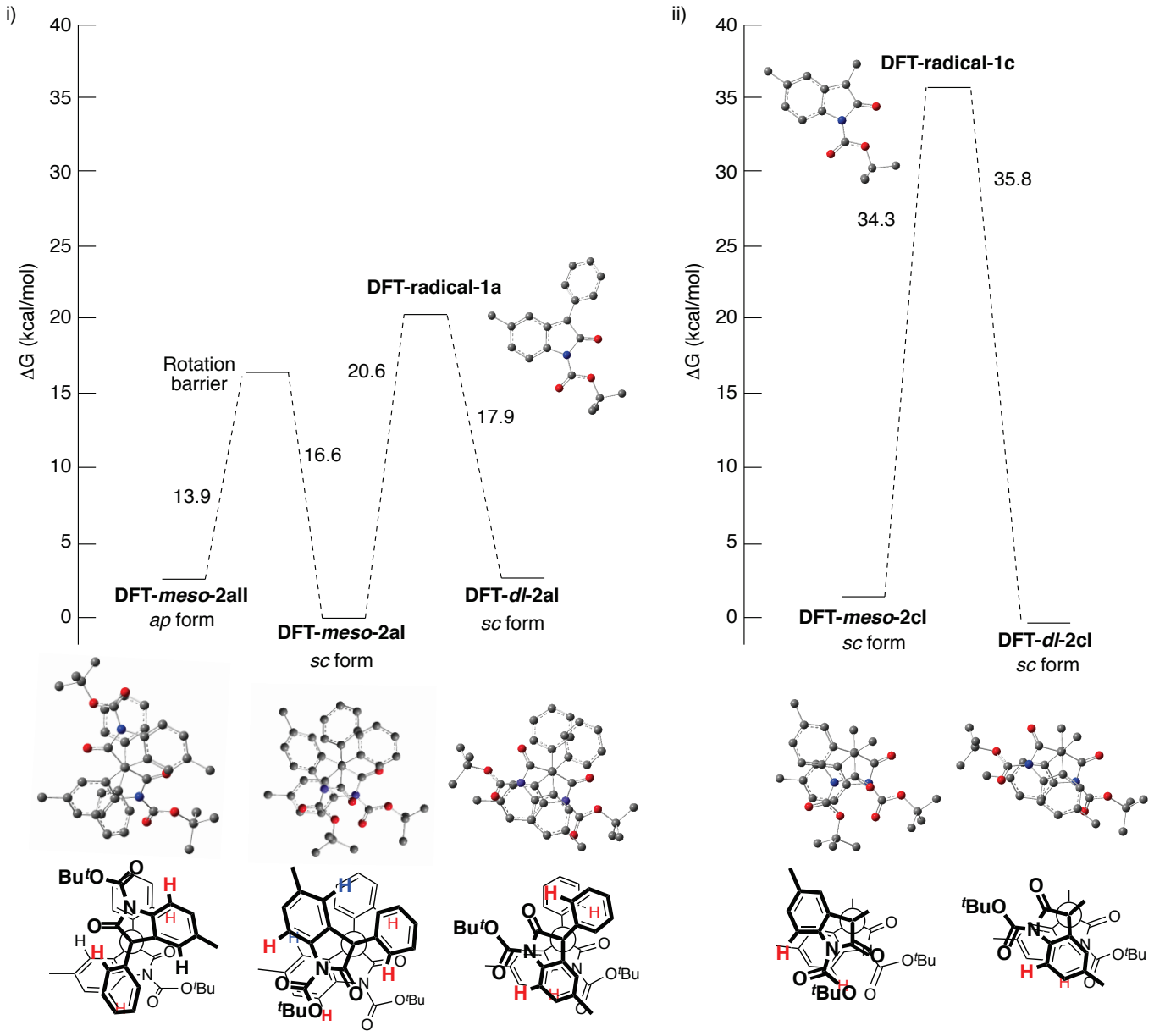

Figure 4. i) Energy diagram for **DFT-*meso*-2aI**, **DFT-*dl*-2aI** and **DFT-radical-1a**; ii) energy diagram for **DFT-*meso*-2cI**, **DFT-*dl*-2cI** and **DFT-radical-1c**. Dimers **2** were computed at the M06-2X/6-311G(d,p) level of theory, while radicals **1** were computed at the UM06-2X/6-311G(d,p) level of theory. All hydrogen atoms in ball illustrations are omitted for the sake of clarity.

On the basis of these findings, we performed similar computational analyses with not only *dl*-**2a** but also *meso*-**2c** and *dl*-**2c** (R^1 = Me, R^2 = Me, P = Boc) (see Supporting Information for details), to gain insight into the mechanism of selective formation of *meso*-**2a**. The energy diagrams of **2a** and **2c**, summarized in Figure 4, illustrate that the BDE values of **2a** [*meso*-**2aI**: 20.6 kcal/mol, *dl*-**2aI**: 17.9 kcal/mol] are significantly smaller than those of **2c** [*meso*-**2cI**: 34.3 kcal/mol, *dl*-**2cI**: 35.8 kcal/mol]. Furthermore, the small BDE and rotation barrier of **2a** can explain why the (±)-*sc* conformation of *meso*-**2a**, which is stabilized by multiple intramolecular CH/O and CH/π interactions, is mainly observed in the dimerization of **1a**.

Table 1. Reaction of **2a** with azo compounds **3**.[a]

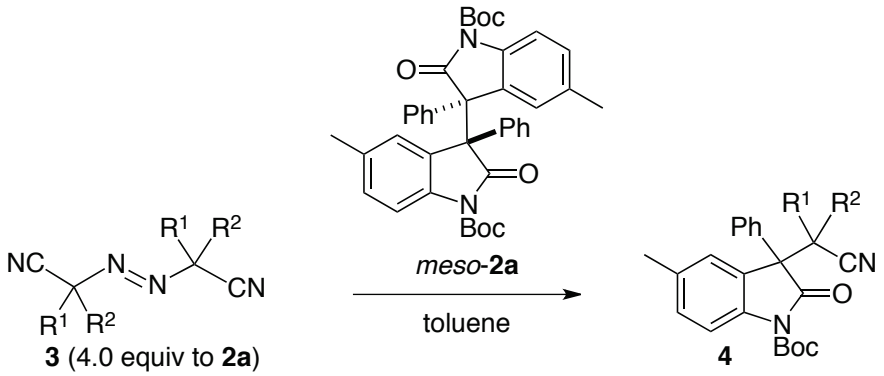

Entry	3	Temp (°C)	Time (h)	4	Yield (%)[b]	dr (%)[c]
1	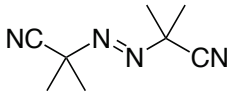	100	0.5	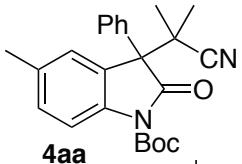	86	---
2		60	15		n.d.	---
	3a: AIBN			**4aa**		
3	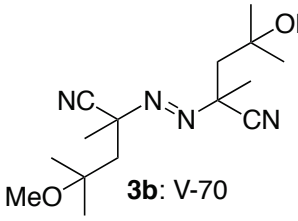	100	0.5	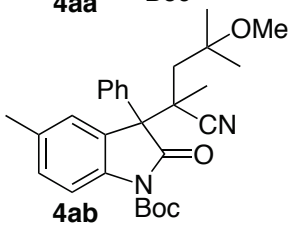	86	1/1
4		40	16		99[d]	1/1
	3b: V-70			**4ab**		
5	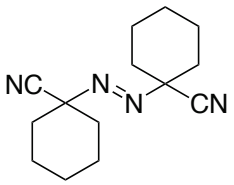	100	2	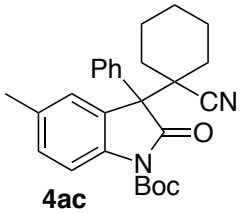	81	---
	3c: V-40			**4ac**		

[a] The reaction was performed on a 0.025 mmol scale. [b] Isolated yield. [c] Determined by ^{1}H NMR using crude mixture. [d] NMR yield determined by CH_2Br_2 as an internal standard.

These experimental results and DFT calculations stimulated us to examine radical-based reactions of *meso*-**2a** aimed at structural diversification. We anticipated that the carbon radical, which can be easily generated from *meso*-**2a** by heating, might serve as an intermediate to construct two distinct contiguous centers by reaction with another radical species.[16] We found that the carbon radicals derived from azo compounds **3** are suitable for constructing two distinct contiguous centers with *meso*-**2a** (Table 1).[17] For example, the reaction of *meso*-**2a** with AIBN (**3a**: azobisisobutyronitrile, $t_{1/2}$= 10 h at 65 °C in toluene) at 100 °C proceeded smoothly to afford the corresponding hetero-coupling product **4aa** in 86% yield (Table 1, entry 1). When we decreased the reaction temperature to 60 °C, formation of **4aa** was not detected (Table 1, entry 2), even when the reaction time was prolonged. Meanwhile, V-70 (**3b**: $t_{1/2}$= 10 h at 30 °C in toluene) is available both at 100 and 40 °C, affording **4ab** in high yields (Table 1, entries 3 and 4). Considering that the monomeric radical can be generated from *meso*-**2a** at lower reaction temperature

than 100 °C, as shown in Figure 1-ii, these results suggest that eliminating nitrogen from the azo compound **3** would initiate the hetero coupling with *meso*-**2a**. The bis-cyclic system having two contiguous quaternary carbon centers was also constructed using V-40 (**3c**: $t_{1/2}$= 10 h at 88 °C in toluene), affording **4ac** in 81% yield (Table 1, entry 5).

In conclusion, a series of solid- and solution-state spectroscopic analyses together with DFT calculations provided mechanistic insights into how the 3-aryl-2-oxindoles **1** selectively generate the *meso*-dimer **2** in oxidative dimerization. We identified crucial roles of the phenyl group at the C(3) position for stabilizing not only *sc* conformation of *meso*-**2a** via cooperative weak CH/O and CH/π interactions, but also the corresponding monomeric carbon radical species in the equilibration. By exploiting the ease of homolysis of the C(3)–C(3') σ-bond in *meso*-**2a**, we successfully trapped the monomeric carbon radical using azo compounds, obtaining **4** with two distinct vicinal all-carbon quaternary centers in high yield. Further efforts to apply our findings to other classes of radical-based transformations are ongoing.

ACKNOWLEDGEMENTS

This work was supported in part by Scientific Research (C) from the MEXT (24550128) and Project Funding from RIKEN. RIKEN HOKUSAI GreatWave provided the computer resources for the DFT calculations.

REFERENCES AND NOTES

1. For a recent review: P. Ruiz-Sanchins, S. A. Savina, F. Albericio, and M. Álvarez, *Chem. Eur. J.*, 2011, **17**, 1388.
2. For reviews: (a) R. Long, J. Huang, J. Gong, and Z. Yang, *Nat. Prod. Rep*., 2015, **32**, 1584; (b) M. A. Schmidt and M. Movassaghi, *Synlett*, 2008, 313; (c) A. Steven and L. E. Overman, *Angew. Chem. Int. Ed*., 2007, **46**, 5488; for a recent example: (d) K. Ohmatsu, N. Inagawa, and T. Ooi, *Nature Chem*., 2014, **6**, 47 and references cited therein.
3. For our review, (a) E. Iwasa, Y. Hamashima, and M. Sodeoka, *Isr. J. Chem*., 2011, **3-4**, 420; for total synthesis of chaetocin: (b) E. Iwasa, Y. Hamashima, S. Fujishiro, E. Higuchi, A. Ito, M. Yoshida, and M. Sodeoka, *J. Am. Chem. Soc*., 2010, **132**, 4078; (c) E. Iwasa, Y. Hamashima, S. Fujishiro, and M. Sodeoka, *Tetrahedron*, 2011, **67**, 6587; for structural and activity relationship: (d) S. Fujishiro, K. Dodo, E. Iwasa, Y. Teng, Y. Sohtome, Y. Hamashima, A. Ito, M. Yoshida, and M. Sodeoka, *Bioorg. Med. Chem. Lett.*, 2013, **23**, 733.
4. Selected examples of oxidative dimerization of **1**: (a) J. Harley-Mason and R. F. Ingleby, *J. Chem. Soc*., 1958, 4782; (b) J. B. Hendrickson, R. Göschke, and R. Ree, *Tetrahedron*, 1964, **20**, 565; (c) A. Inada and Y. Morita, *Heterocycles*, 1982, **19**, 2139; (d) T. Kato, A. Inada, Y. Morita, and H.

Miyamae, *Chem. Pharm. Bull*.,1985, **33**, 5270; (e) T. Suyama, T. Kato, Y. Morita, and H. Miyamae, *Heterocycles*, 1994, **37**, 1069; (f) C.-L. Fang, S. Horne, N. Taylor, and R. Rodrigo, *J. Am. Chem. Soc*., 1994, **116**, 9480; (g) H. J. Lee, S. Lee, J. W. Lim, and J. N. Kim, *Bull. Korean Chem. Soc.*, 2013, **34**, 2446; (h) S. Ghosh, S. Chaudhuri, and A. Bisai, *Org. Lett*., 2015, **17**, 1373; (i) T. Bleith, Q.-H. Deng, H. Wadepohl, and L. H. Gade, *Angew. Chem. Int. Ed*., 2016, **55**, 7852; (j) H.-R. Wu, H.-Y. Huang, C-L. Ren, L. Liu, D. Wang, and C.-J. Li, *Chem. Eur. J*., 2015, **21**, 16744; (k) H.-R. Wu, L. Cheng, D.-L. Kong, H.-Y. Huang, C.-L. Gu, L. Liu, D. Wang, and C.-J. Li, *Org. Lett*., 2016, **18**, 1382.

5. Photocatalytic dimerization for synthesis of **2**: W.-L. Jia, J. He, J.-J. Yang, X.-W. Gao, Q. Liu, and L.-Z. Wu, *J. Org. Chem*., 2016, **81**, 7172.
6. For other approaches to synthesis of **2**: (a) H. Mitsunuma, M. Shibasaki, M. Kanai, and S. Matsunaga, *Angew. Chem. Int. Ed*., 2012, **51**, 5217; (b) B. M. Trost and M. Osipov, *Angew. Chem. Int. Ed*., 2013, **52**, 9176.
7. For catalytic sequential intramolecular arylation/oxidative dimerization for synthesis of **2**: (a) S. Ghosh, S. De, B. N. Kakde, S. Bhunia, A. Adhikary, and A. Bisai, *Org. Lett*., 2002, **14**, 5864; for a diastereoselective version using chiral **1**: (b) X. Shen, Y. Zhou, Y. Xi, J. Zhao, and H. Zhang, *Chem. Commun*., 2015, **51**, 14873.
8. 'International Tables for Crystallography', **C**, Table 9.5.1.1., ed. by A. J. C. Wilson, Kluwer Academic Publishers, Dordrecht, 1992.
9. Quite recently, Gade and co-workers reported the use of *meso*-dimer **2** for alkylation reaction, showing significant reversibility of *meso*-**2** formation: see, ref 4i and details in the Supporting Information.
10. Recent reviews of CH/O interactions: (a) G. R. Desiraju, *Acc. Chem. Res.*, 1996, **29**, 441; (b) T. Steiner, *Angew. Chem. Int. Ed.*, 2002, **41**, 48; (c) O. Takahashi, Y. Kohno, and M. Nishio, *Chem. Rev*., 2010, **110**, 6049.
11. Recent reviews of CH/π interactions, see as well as refs. 10b and 10c: (a) M. Nishio, *Phys. Chem. Chem. Phys*., 2011, **13**, 13873; (b) M. Nishiro, M. Hirota, and Y. Umezawa, 'The CH/Interaction: Evidence, Nature, and Consequence (Methods in Stereochemical Analysis)' ed. by A. P. Marchand, Wiley-VCH, 1998.
12. Y. Hamashima, T. Suzuki, H. Takano, Y. Shimura, and M. Sodeoka, *J. Am. Chem. Soc*., 2005, **127**, 10164.
13. For selected examples of detection of the carbon radical derived from benzofuranones by UV-Vis spectroscopy: (a) H. H. Wasserman, T.-C. Liu, and E. R. Wasserman, *J. Am. Chem. Soc*., 1953, **75**, 2056; (b) J. C. Scaiano, A. Martin, G. P. A. Yap, and K. U. Ingold, *Org. Lett*., 2000, **2**, 899; (c) M.

Frenette, C. Aliaga, E. Font-Sanchis, and J. C. Scaiano, *Org. Lett*., 2004, **6**, 2579; (d) K. Imato, A. Irie, T. Kosuge, T. Ohishi, M. Nishihara, A. Takahara, and H. Otsuka, *Angew. Chem. Int. Ed.*, 2014, **54**, 6168.

14. M. J. Frisch, *et al*., Gaussian 09, revision C.01 (Gaussian, Inc.: Wallingford, CT, 2010).
15. Y. Zhao and D. G. Truhlar, *Acc. Chem. Res*., 2008, **41**, 157.
16. T. H. Koch, J. A. Olesen, and J. DeNiro, *J. Am. Chem. Soc*., 1975, **97**, 7285.
17. When we used TEMPO (2,2,6,6-tetramethylpiperidine 1-oxyl) as a radical-trapping reagent in toluene at 100 °C, *meso*-**2a** was mainly recovered and no cross-coupling products were detected.